Available online at www.sciencedirect.com
SCIENCE DIRECT®
ELSEVIER
Nuclear Physics A 736 (2004) 269–279
NUCLEAR PHYSICS A
www.elsevier.com/locate/npe

Band crossing and the $N = 7$ intruder orbital in superdeformed nucleus ^{193}Hg

S.X. Liu *, J.Y. Zeng

School of Physics, Peking University, Beijing 100871, China

Received 10 February 2004; accepted 16 March 2004

Abstract

The particle-number conserving method for treating the cranked shell model with monopole and quadrupole pairing interactions is used to investigate the microscopic mechanism of six superdeformed bands in ^{193}Hg, including the occupation probability of each cranked orbital, the contributions to angular momentum alignment from the direct contributions $j_x(\mu)$ of the particle in orbital μ, and the interference contribution $j_x(\mu\nu)$ from the particles in orbitals μ and ν. Our calculated results support the previous assignments of configuration of six superdeformed bands in ^{193}Hg and provide a satisfactory demonstration for the crucial role of the high-N intruder orbital $\nu[761]3/2$ in band crossing and angular momentum alignment.

PACS: 21.10.Re; 21.60.Cs; 27.80.+w

Keywords: Superdeformed band; Band crossing; High-N intruder orbital; Particle-number conserving method

1. Introduction

An impressive experimental and theoretical effort has been devoted to determine the intrinsic states on which superdeformed (SD) rotational bands are built. In the mass $A \sim 190$ region, the study of several odd-neutron SD nuclei has revealed many excited SD bands which have been interpreted in terms of individual excitations of the valence neutron around the Fermi surface. Among these SD nuclei, the nucleus ^{193}Hg is the most spectacular example of SD nuclear structure. Up to six SD bands have been observed in this nucleus providing a wealth of nuclear structure information involving band crossing

* Corresponding author.
E-mail address: liusx@pku.edu.cn (S.X. Liu).

0375-9474/$ – see front matter
doi:10.1016/j.nuclphysa.2004.03.036

[1], cross-talk between bands [1–3], identical bands [4,5], and the neutron $N = 7$ intruder orbital [6]. These data have helped to establish the nature of single-neutron orbitals around the SD shell closure at $N = 112$. From the observation of cross-talk M1 transitions between SD bands in ^{193}Hg and by comparison to theoretical calculations [7], the occupancy of the two high Ω neutron orbitals [512]5/2 and [624]9/2 has been clearly shown. However, the alignment of the $N = 7$ orbitals is observed to be reduced in comparison with the Woods–Saxon calculations. On the other hand, the Hartree–Fock calculations predict slightly too weak Coriolis coupling. This may suggest that the relative placement of the $[761]3/2^-$ and $[752]5/2^-$ orbitals with respect to the $N = 113$ Fermi level should be slightly modified in both models [6].

The fascinating phenomenon of identical bands have generated a great deal of theoretical interest and activity aimed at understanding the underlying mechanism. The set of identical SD bands, $^{192}\mathrm{Hg}(1)$, $^{193}\mathrm{Hg}(2\mathrm{a})$, $^{193}\mathrm{Hg}(2\mathrm{b}, 3)$ and $^{194}\mathrm{Hg}(2, 3)$ are interpreted as bands based on 0-quasiparticle (qp), 1-qp $\nu[512]5/2(\alpha = +1/2)$, $\nu[624]9/2(\alpha = \pm 1/2)$ and 2-qp $\nu[512]5/2[624]9/2(\alpha = 0, 1)$ states, respectively, [6,8]. The experimental ω variation of both $J^{(1)}$ and $J^{(2)}$ for these identical SD bands are reproduced quite well by a particle-number conserving (PNC) treatment for the cranked shell model (CSM), in which the blocking effect is taken into account exactly and no free parameter is involved [9]. Our PNC calculations present the first precise quantitative explanation for microscopic mechanism of identical SD bands in the $A \sim 190$ region. Both the similarity and difference in the ω variation of $J^{(1)}$ and $J^{(2)}$ between these identical SD bands and the identical ND bands in rare-earth nuclei are explained consistently. A strict and consistent treatment of the blocking effect on pairing is crucial to account for these identical bands. Moreover, blocking effects are especially important for treating high-K multi-qp bands widely observed in the ND rare-earth nuclei.

In Ref. [10], the cranked Hartree–Fock–Bogoliubov (HFB) method is applied to the study of six SD bands observed in ^{193}Hg. Their results support the assignation of these bands to specific 1-qp excitations with respect to ^{192}Hg and also show that pairing correlations are not significantly reduced by the creation of 1-qp. However, the interaction between the negative parity negative signature bands found experimentally is not reproduced by the self-consistent 1-qp excited HFB calculation. In addition, the cranking calculations using a Woods–Saxon potential have shown that the use of the Lipkin–Nogami prescription for projecting good particle number and the inclusion of quadrupole pairing fields have a remarkable improvement in the description of the yrast SD bands of even–even Hg and Pb isotopes from $N = 110$–116 [11]. In this paper we adopt a PNC treatment for the CSM including both monopole and quadrupole pairing interactions to investigate the six SD bands in ^{193}Hg. A satisfactory explanation for the band crossing and alignment of the neutron $N = 7$ intruder orbital is provided by our PNC calculation in which the strength of pairing interaction keeps unchanged.

2. PNC method

The CSM Hamiltonian with pairing interactions is

$$H_{\mathrm{CSM}} = H_{\mathrm{SP}} - \omega J_x + H_P = H_0 + H_P, \tag{1}$$

where $H_0 = H_{\mathrm{SP}} - \omega J_x = \sum_i h_0(\omega)_i$, $h_0(\omega) = h_{\mathrm{Nilsson}} - \omega j_x$, is the one-body part of H_{CSM}, h_{Nilsson} the Nilsson Hamiltonian, $-\omega J_x$ the Coriolis interaction and H_P the pairing interaction including both the monopole and quadrupole pairing interactions [12,13]. The Nilsson (modified oscillator) potential has been quite successful in describing the properties of SD bands [14–16]. In the PNC treatment, first, $h_0(\omega)$ is diagonalized to obtain the cranked Nilsson orbitals. Then, H_{CSM} is diagonalized in a sufficiently large cranked many-particle configuration (CMPC) space to obtain the yrast and low-lying eigenstates. For the details of PNC method, see Refs. [17,18]. Assuming an eigenstate of H_{CSM} is expressed in terms of the CMPC's:

$$|\psi\rangle = \sum_i C_i |i\rangle, \tag{2}$$

where $|i\rangle$ denotes an occupation of particles in cranked orbitals and C_i is the corresponding probability amplitude. The occupation probability of the cranked orbital μ (including both signature $\alpha = \pm 1/2$) is

$$n_\mu = \sum_i |C_i|^2 P_{i\mu}, \quad P_{i\mu} = \begin{cases} 1, & \text{if } |\mu\rangle \text{ is occupied in the CMPC } |i\rangle, \\ 0, & \text{otherwise.} \end{cases} \tag{3}$$

The angular momentum alignment for the state $|\psi\rangle$ is $\langle J_x\rangle = \langle\psi|J_x|\psi\rangle$, and the kinematic moment of inertia of is $J^{(1)} = \langle J_x\rangle/\omega$. Because J_x is a one-body operator, $\langle i|J_x|j\rangle$ for $i \neq j$ does not vanish only when $|i\rangle$ and $|j\rangle$ differ by one particle occupation. Supposing after a certain permutation of creation operators, $|i\rangle$ and $|j\rangle$ are brought into the forms

$$|i\rangle = (-)^{M_{i\mu}}|\mu\cdots\rangle, \qquad |j\rangle = (-)^{M_{j\nu}}|\nu\cdots\rangle, \tag{4}$$

where the ellipsis stands for the same particle occupation and $(-)^{M_{i\mu}} = \pm 1$, $(-)^{M_{j\nu}} = \pm 1$ according to whether the permutation is even or odd. Therefore the angular momentum alignment of the state $|\psi\rangle$ is

$$\langle J_x\rangle = \sum_\mu j_x(\mu) + \sum_{\mu<\nu} j_x(\mu\nu), \tag{5}$$

$$j_x(\mu) = \langle\mu|j_x|\mu\rangle n_\mu,$$
$$j_x(\mu\nu) = 2\langle\mu|j_x|\nu\rangle \sum_{i<j} (-)^{M_{i\mu}+M_{j\nu}} C_i C_j \quad (\mu \neq \nu), \tag{6}$$

where $j_x(\mu)$ is the direct contribution to $\langle J_x\rangle$ from a particle occupying the cranked orbital μ and $j_x(\mu\nu)$ is the contribution to $\langle J_x\rangle$ from the interference between two particles occupying the cranked orbitals μ and ν, which has no counterpart in the mean-field (BCS) treatment. Calculations show that $j_x(\mu\nu)$ plays an important role for the odd–even difference and nonadditivity in moment of inertia. The expression for dynamic moment of inertia $J^{(2)} = \frac{d}{d\omega}\langle J_x\rangle$ is similar.

3. Theoretical calculations and discussion

For most SD bands in the $A \sim 190$ region, the spins have not been established, thus only $J^{(2)}$ can be extracted from the experimental differences in γ transition energies,

$J^{(2)}(I) = 4\hbar^2/[E_\gamma(I+2 \to I) - (E_\gamma(I \to I-2)]$. Fortunately, because of the regular behavior of E_γ, their spins have been consistently and reliably predicted by various approaches [19]. Moreover, the spins of some SD bands (^{194}Hg(1), ^{194}Hg(3), ^{194}Pb(1), ^{193}Tl(1, 2), etc.) have been established experimentally [20], which are in agreement with the prediction. Thus, the kinematic Moment of inertia $J^{(1)}$ may be extracted by the experimental γ transition energies themselves, $J^{(1)}(I) = (2I+1)\hbar^2/E_\gamma(I+1 \to I-1)$, which is much more accurate than $J^{(2)}$ extracted by the difference in γ transition energies.

For ND bands in the rare-earth nuclei, the pairing interaction strengths are determined by the experimentally odd–even differences in binding energies and bandhead moments of inertia, but for SD bands in the $A \sim 190$ region, no experimental binding energies are available. Because the spins of ^{194}Hg(3) have been established experimentally, in our PNC calculation the sixteen accurate $J^{(1)}(\omega)$ data ($\hbar\omega \approx 0.10$–0.40 MeV) of ^{194}Hg(3) are used to determine the effective pairing strengths, which are then adopted to calculate the moments of inertia of the six SD bands in neighboring nucleus ^{193}Hg. The effective pairing interaction strength depends on the dimension of the truncated CMPC space. In the following calculations, the dimension of CMPC space is about 900 for proton and 1000 for neutron. For the yrast and low-lying excited states, the number of main CMPC (weight $> 10^{-2}$) is very limited (~ 20) and all of them and almost all of CMPC with *weigtht* $> 10^{-3}$ have been included in this truncated CMPC space, so the obtained solutions to the low-lying eigenstates are quite accurate. In such a truncated CMPC space, the effective monopole and quadrupole pairing strengths (in units of MeV) are: $G_0 = 0.300$, $G_2 = 0.065$ for proton, $G_0 = 0.205$, $G_2 = 0.003$ for neutron.

In our PNC calculation, the Nilsson parameters (κ, μ) are taken from the Lund systematics [21] and the deformation parameters $(\varepsilon_2, \varepsilon_4)$ are taken from the Ref. [8]. A minor adjustment for the deformation parameters of SD bands ^{193}Hg$(1, 5)$ is made because both bands are based on a deformation-driving high-N orbital. Neutron cranked single-particle level diagram is plotted in Fig. 1 for a large prolate deformation ($\varepsilon_2 = 0.45$, $\varepsilon_4 = 0.025$). The corresponding Woods–Saxon single-particle diagram is similar to those shown in Fig. 1 as far as the placing of the high-N intruder orbitals is concerned. One difference is that the $N = 112$ gap does not show up in our calculations, but instead there is a small gap at $N = 114$. For the six SD bands in ^{193}Hg, experimental and theoretical effort leads to the conclusion that two pairs of signature partner bands are based on the $[512]5/2^-$ and $[624]9/2^+$ neutron orbitals. Other two SD bands was considered to be based on the $j_{15/2}$ single-particle configurations ($[761]3/2^-$ or $[752]5/2^-$) [6]. Our PNC calculations obviously support the assignation of $[761]3/2^-$ neutron intruder orbital for the two SD bans. Then, at low rotational frequencies the six SD bands in ^{193}Hg have the following configuration: band 1 is $\nu[512]5/2(\alpha = -1/2)$, band 2a is $\nu[512]5/2(\alpha = +1/2)$, band 3 is $\nu[624]9/2(\alpha = -1/2)$, band 2b is $\nu[624]9/2(\alpha = +1/2)$, band 4 is the favoured $\nu[761]3/2(\alpha = -1/2)$ and band 5 is the unfavoured $\nu[761]3/2(\alpha = +1/2)$.

In Fig. 2 are shown the experimental and calculated $J^{(1)}$ and $J^{(2)}$ of ^{193}Hg(1, 2a, 2b, 3). The dynamic moments of inertia of ^{193}Hg(2a, 2b, 3) are identical with those of ^{194}Hg(2, 3), because they are all based on two strongly coupled neutron orbitals [512]5/2 and [624]9/2 (for the details of microscopic mechanism of those identical SD bands, see Ref. [9]). For ^{193}Hg(1), the experimental and calculated results show that at $\hbar\omega \approx 0.27$ MeV, the alignment of ^{193}Hg(1) has a sudden increase as an evidence of band crossing between

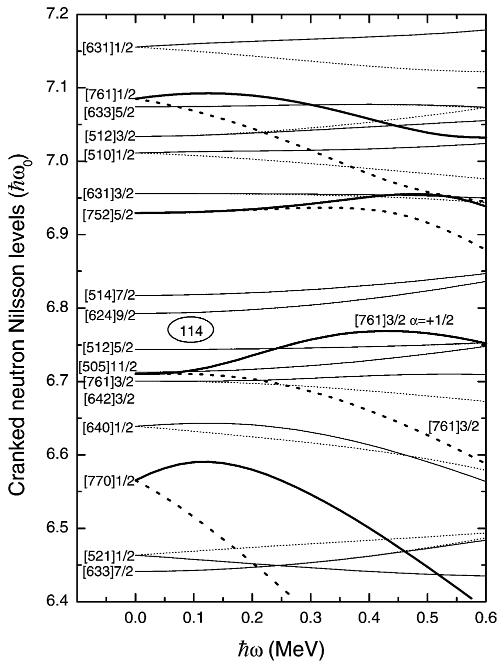

Fig. 1. Cranked neutron Nilsson orbitals energies near the Fermi surface of ^{193}Hg. The signature $\alpha = \pm 1/2$ orbitals are denoted by solid and dotted lines, respectively. The high j intruder orbitals are denoted by bold lines.

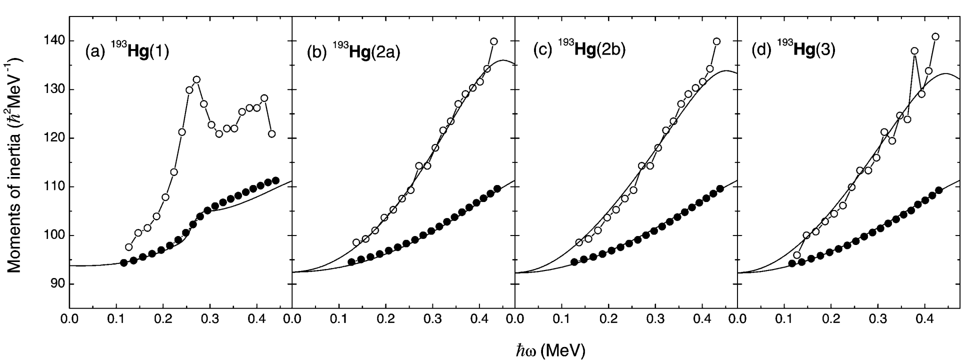

Fig. 2. Experimental and calculated $J^{(1)}$ and $J^{(2)}$ of the SD bands, ^{193}Hg(1, 2a, 2b, 3). The experimental $J^{(1)}$ and $J^{(2)}$ of ^{193}Hg(1, 2a, 2b, 3) are denoted by solid and open circles, respectively, and the calculated results are denoted by lines. (a) ^{193}Hg(1), (b) ^{193}Hg(2a), (c) ^{193}Hg(2b), (d) ^{193}Hg(3).

^{193}Hg(1) and ^{193}Hg(4). This crossing is interpreted as the crossing between $N = 5$ and $N = 7$ orbitals, where the configurations of two SD bands are interchanged. This scenario is consistent with the distribution and ω variation of neutron orbitals near Fermi surface of ^{193}Hg (see Fig. 1). It is seen that while the orbital $\nu[512]5/2$ remains almost unchanged with ω, the intruder orbital $\nu[761]3/2$ has a large signature splitting with the

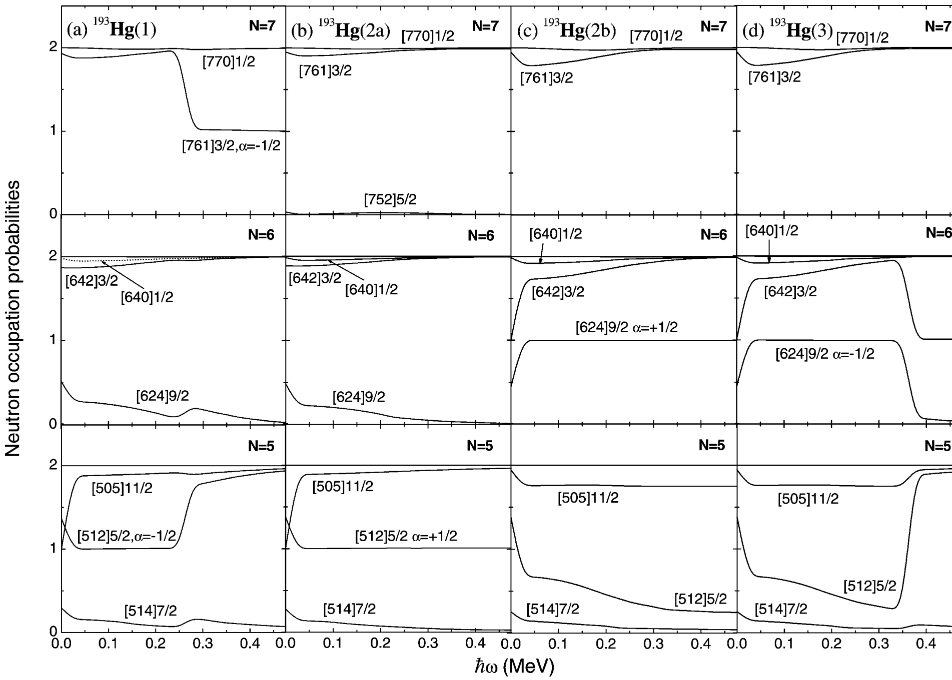

Fig. 3. Occupation probability n_μ of each orbital μ (including both $\alpha = \pm 1/2$) near the Fermi surface for the SD bands, ^{193}Hg(1, 2a, 2b, 3). Occupation probability of each orbital for the same SD band is placed in the one column. (a) ^{193}Hg(1), (b) ^{193}Hg(2a), (c) ^{193}Hg(2b), (d) ^{193}Hg(3).

$\alpha = -1/2$ being favoured. The unfavoured $\nu[761]3/2(\alpha = +1/2)$ orbital below $\nu[512]5/2$ at low frequencies rises quickly with ω and crosses with $\nu[512]5/2$ at $\hbar\omega \approx 0.25$ MeV. For ^{193}Hg(1) ($\alpha = -1/2$) before band crossing, the orbital $\nu[512]5/2(\alpha = +1/2)$ is empty and both the orbitals $\nu[761]3/2(\alpha = \pm 1/2)$ are occupied. After band crossing the particle occupying $\nu[761]3/2(\alpha = +1/2)$ will jump to $\nu[512]5/2(\alpha = +1/2)$. However, this band crossing cannot occur for ^{193}Hg(2a) ($\nu[512]5/2$, $\alpha = +1/2$), because the orbital $\nu[512]5/2(\alpha = +1/2)$ is always occupied.

The configurations and the ω variation of neutron occupation probabilities of ^{193}Hg(1, 2a, 2b, 3) are clearly shown in Fig. 3. For band 1, at low ω, the occupation probability of $\nu[512]5/2$, $n_\mu \approx 1$ show that one neutron occupies the $\nu[512]5/2(\alpha = -1/2)$ orbital and another orbital ($\alpha = +1/2$) is empty. This situation almost keeps unchanged with ω until $\hbar\omega \approx 0.27$ MeV, after which the occupation probabilities of $\nu[512]5/2$ and $\nu[761]3/2$ are interchanged, which implies the occurrence of a band crossing. On the contrary, the occupation probabilities of band 2a and 2b are much more simple, i.e., except that the occupation probabilities $n_\mu \approx 1$ for the two orbitals [512]5/2 and [624]9/2, other neutron orbitals (including high-N intruder orbitals)l are nearly occupied or empty. For band 3, an interchange of configurations among the neutron [624]9/2, [642]3/2 and [512]5/2 orbitals occurs at $\hbar\omega \approx 0.35$ MeV, the anomalous behavior of dynamic moment of inertia of band 3 at higher ω seems to reflect this change of configurations, but the crossing is of weak

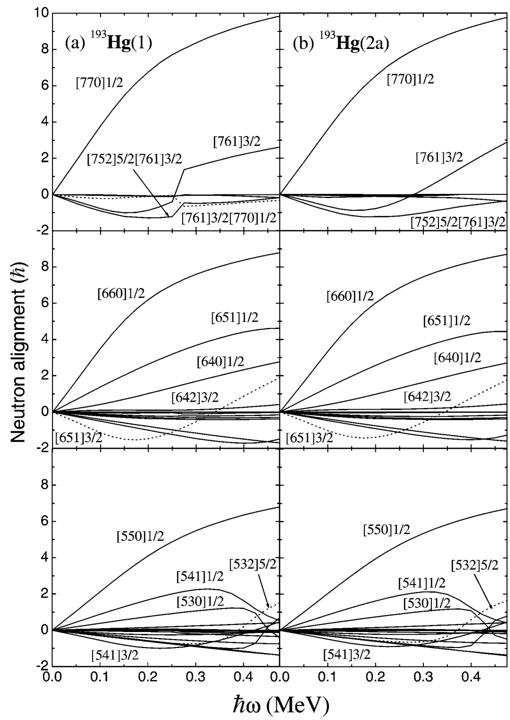

Fig. 4. The direct contributions to $\langle J_x \rangle$ from the particle in cranked orbital μ, $j_x(\mu)$ and the interference contribution $j_x(\mu\nu)$ between cranked orbitals μ and ν for the SD bands, $^{193}\mathrm{Hg}(1, 2\mathrm{a})$. (a) ^{193}Hg(1), (b) ^{193}Hg(2a).

interaction [22]. A strong interaction between band 1 and 4 is observed experimentally ($V_{\mathrm{int}} \approx 26$ keV [1] or 42 keV [22] from a simple two-level mixing calculation), we wonder whether this strong interaction arises from the interchange of configurations between different main shells ($N = 5$ and 7).

More detailed informations come from the single-particle contributions to angular momentum alignment in Fig. 4. High-j low-ω orbitals are characterized by their large contributions to alignment and large Coriolis responses. Thus the change of alignment in band crossing is mainly attributed to the change of high-N configuration, and the crossing of band 1 and 4 may serve as a typical example. According to our PNC calculations, in the region of band crossing, the total increase of alignment of band 1 is $3.2\hbar$ (the average increase of alignment $1.6\hbar$ is included). The direct contribution of $[761]3/2$ is $1.8\hbar$, the contributions of the interference terms, $[761]3/2[770]1/2$ and $[752]5/2[761]3/2$ are $-0.6\hbar$ and $0.8\hbar$, respectively. Calculations show that the contribution from band crossing ($\sim 1.6\hbar$) mainly comes from the intruder $N = 7$ shell ($\sim 2.0\hbar$), and a minor contribution ($\sim -0.4\hbar$) comes from $N = 5, 6$ shells. The large contributions to moment of inertia from high-j low-ω orbitals are more clearly shown in Fig. 5 for band 2b and 3. In fact, the three bands, 2a, 2b and 3 have almost the same alignment.

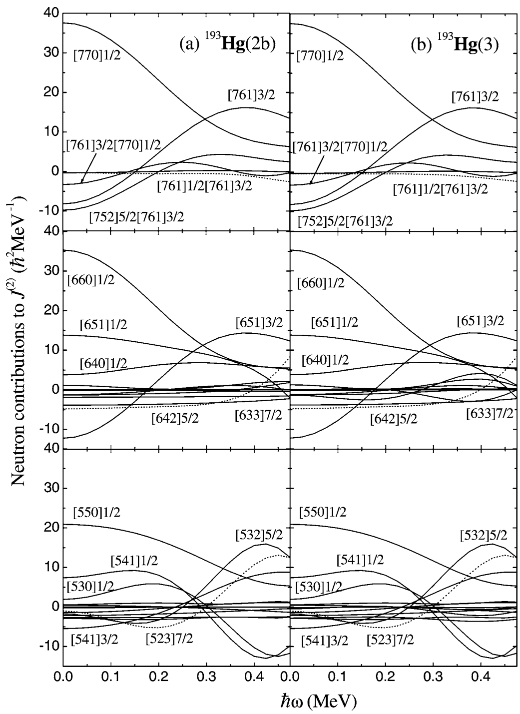

Fig. 5. The direct contributions to $J^{(2)}$ from the particle in cranked orbital μ, $j^{(2)}(\mu)$ and the interference contribution $j^{(2)}(\mu\nu)$ between cranked orbitals μ and ν, for the SD bands, ^{193}Hg$(2\text{b}, 3)$. (a) ^{193}Hg(2b), (b) ^{193}Hg(3).

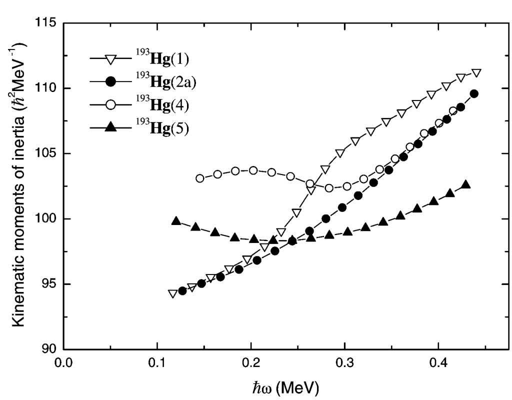

Fig. 6. Experimental $J^{(1)}$ of the SD bands, ^{193}Hg$(1, 2\text{a}, 4, 5)$.

The calculations of band 4 and 5 involving the high-N intruder orbitals are more difficult in general because the corresponding orbitals have large signature splitting and are deformation-driving. In Fig. 6, we plot the experimental kinematic moments of inertia of ^{193}Hg$(1, 2\text{a}, 4, 5)$ with rotational frequencies ω, in which their spins have been proposed

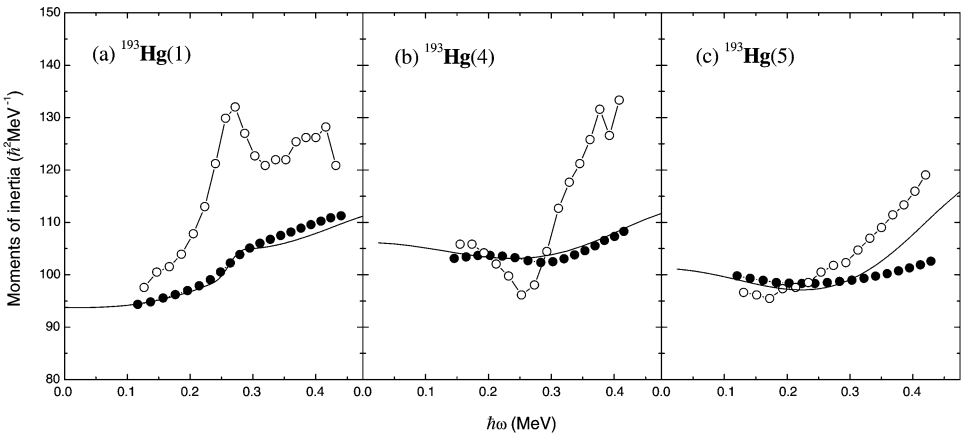

Fig. 7. Same as Fig. 2, for ^{193}Hg$(1, 4, 5)$.

reliably and consistently according to our procedure of spin assignment [19] and are in agreement with the spin assignments of Ref. [6]. For most SD bands in the $A \sim 190$ region, both $J^{(2)}$ and $J^{(1)}$ moments of inertia exhibit the same smooth rise with rotational frequencies. The SD bands, ^{193}Hg$(2a, 2b, 3)$ are such typical examples, their alignments and corresponding variation with rotational frequencies are almost identical because they all are based on the strongly coupled neutron orbitals. The signature splitting of $\nu[761]3/2$ has the effect of further increasing the moments of inertia for the favoured branch and decreasing those for the unfavoured branch [6]. The odd–even difference in moments of inertia at low ω limit is the manifestation of blocking effects on pairing, but with increasing ω the blocking effect gradually weakens due to very strong Coriolis anti-pairing interaction, the odd–even difference gradually disappears [9,19]. Thus, at low ω limit, the moments of inertia of bands 4 and 5 tend to the same value, which is much larger than that of ^{193}Hg(2a). In contrast, at higher rotational frequencies, the experimental kinematic moments of inertia of bands 1 and 5 have a large signature splitting and both bands obviously deviate from that of ^{193}Hg(2a) (see Fig. 6).

The results of our PNC calculations about band 4 and 5 in Fig. 7 are also very satisfactory. The neutron occupation probabilities of these bands are shown in Fig. 8. More revealing is the comparison between the experimental alignments for the bands ^{193}Hg$(1, 5)$ and the calculated alignments for the proposed single-particle configurations. The band 2a is taken as a reference that represent the average smooth increasing of angular momentum alignment (see Fig. 6). In this comparison, we select a higher rotational frequency at $\hbar\omega \approx 0.3$ MeV, the best point at which, according to experimental data and our PNC calculations, three bands have very pure configurations (see Figs. 3 and 8), and blocking effect could be neglected at such a higher ω. The experimental (calculated) alignments for band 1 and 5 relative to band 2a are $1.31\hbar$ $(1.27\hbar)$ and $-0.62\hbar$ $(-0.37\hbar)$, respectively, and a remarkable agreement can be seen. In fact, the corresponding calculated alignments of contributions from the major shell $N = 7$ are $1.49\hbar$ and $-1.12\hbar$, respectively. The discrepancy between the relative alignments of $N = 7$ shell and the total alignment should come from the deformation effect and alignments from other neutron and proton shells. It

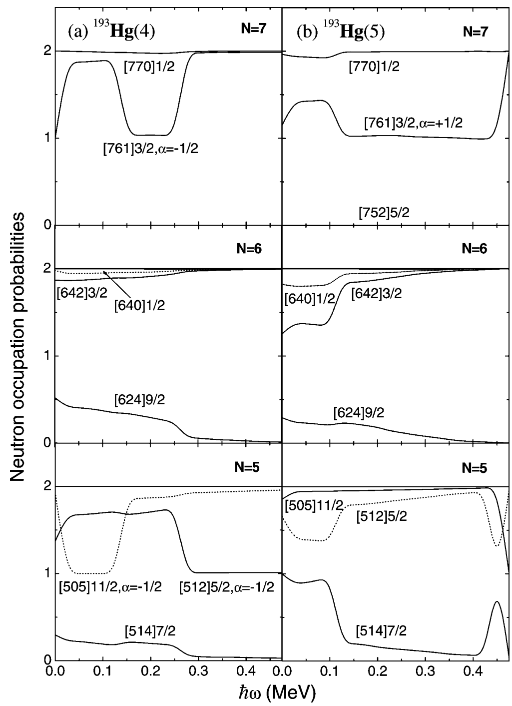

Fig. 8. Same as Fig. 3, for ^{193}Hg(4, 5).

is worthy to note that the SD bands 1 and 4 in ^{191}Hg have properties similar to those of ^{193}Hg(1, 5) and these bands are believed to be built on the same orbital ν[761]3/2 [23]. In the vicinity of $N = 111$, from ^{189}Hg to ^{193}Hg, we believe that the high-N intruder orbital [761]3/2 play a central role on the anomalous behavior of dynamic moment of inertia and band crossing [24].

4. Summary

Our PNC calculations provide a reliable explanation for the microscopic mechanism of the six SD bands in ^{193}Hg, in which the high-N intruder orbital ν[761]3/2 plays a crucial role in band crossing and angular momentum alignment. From our calculation, we may further conclude that the high-N intruder orbital ν[761]3/2 should be responsible for the anomalous behavior of dynamic moment of inertia and band crossing in the vicinity of $N = 111$, from ^{189}Hg to ^{193}Hg. Because the high-N intruder orbital ν[761]3/2 is deformation-driving, the calculated results are expected to be improved if the change of deformation with rotational frequencies is considered.

Acknowledgements

This work is supported by National Natural Science Foundation of China under Project 10375001.

References

[1] D.M. Cullen, et al., Phys. Rev. Lett. 65 (1990) 1547.
[2] P. Fallon, et al., Phys. Rev. Lett. 70 (1993) 2690.
[3] M.J. Joyce, et al., Phys. Rev. Lett. 71 (1993) 2176.
[4] E.A. Henry, et al., Z. Phys. A 335 (1990) 361.
[5] F.S. Stephens, et al., Phys. Rev. Lett. 65 (1990) 301.
[6] M.J. Joyce, et al., Phys. Lett. B 340 (1994) 150, and references therein.
[7] P.B. Semmes, I. Ragnarsson, S. Åberg, Phys. Lett. B 345 (1995) 185.
[8] M.A. Riley, et al., Nucl. Phys. A 512 (1990) 178.
[9] S.X. Liu, J.Y. Zeng, E.G. Zhao, Phys. Rev. C 66 (2002) 024320.
[10] P.-H. Heenen, P. Bonche, H. Flocard, Nucl. Phys. A 588 (1995) 490.
[11] W. Satula, R. Wyss, Phys. Rev. C 50 (1994) 2888.
[12] M. Wakai, A. Faessler, Nucl. Phys. A 295 (1978) 86.
[13] M. Dibel, Nucl. Phys. A 419 (1984) 221.
[14] I. Ragnarsson, Nucl. Phys. A 557 (1993) 167c.
[15] L.B. Karlsson, I. Ragnarsson, S. Åberg, Nucl. Phys. A 639 (1998) 654.
[16] A.V. Afanasjev, I. Ragnarsson, P. Ring, Phys. Rev. C 59 (1999) 3166.
[17] J.Y. Zeng, Y.A. Lei, T.H. Jin, Z.J. Zhao, Phys. Rev. C 50 (1994) 746.
[18] X.B. Xin, et al., Phys. Rev. C 62 (2000) 067303.
[19] S.X. Liu, J.Y. Zeng, Phys. Rev. C 58 (1998) 3266, and references therein.
[20] S. Bouneau, et al., Eur. Phys. J. A 2 (1998) 245.
[21] T. Bengtsson, I. Ragnarsson, Nucl. Phys. A 436 (1985) 14.
[22] S.X. Liu, X.B. Xin, Y.A. Lei, J.Y. Zeng, J. Phys. G 26 (2000) 79.
[23] M.P. Carpenter, et al., Phys. Rev. C 51 (1995) 2400.
[24] R.B. Firestone, S.Y. Frank Chu, C.M. Baglin (Eds.), Table of Isotopes, Wiley, New York, 1998.